Phytochemistry 253 (2027) 115066

Contents lists available at ScienceDirect

Phytochemistry

journal homepage: www.elsevier.com/locate/phytochem

Bioactive natural compounds from the widely distributed, diverse root endophytic fungal genus *Darksidea*

Péter János Berek-Nagy [a], Dániel G. Knapp [a,b], Márta Kraszni [c,d], Gergő Tóth [c,d], Sándor Csíkos [a], Petra Lengyel [a], Orsolya Dobay [e], Galiya K. Akhmetova [a,f], Aldabergen Kiyas [f], Vladimir Zabolotskich [f], Jose G. Maciá-Vicente [g], María-José Romero-Jiménez [h], Andrea Porras-Alfaro [i], Iñigo Zabalgogeazcoa [j], Gábor M. Kovács [a,k,*,1], Imre Boldizsár [a,d,l,**,1]

[a] *Department of Plant Anatomy, Institute of Biology, Eötvös Loránd University, Pázmány Péter sétány 1/C, Budapest, 1117, Hungary*
[b] *Department of Forestry and Wood Technology, Linnaeus University, Växjö, Sweden*
[c] *Department of Pharmaceutical Chemistry, Semmelweis University, Hőgyes Endre u. 9, Budapest, 1092, Hungary*
[d] *Center for Pharmacology and Drug Research & Development, Semmelweis University, Budapest, 1085, Hungary*
[e] *Institute of Medical Microbiology, Semmelweis University, Nagyvárad tér 4, Budapest, 1089, Hungary*
[f] *A. I. Barayev Research and Production Centre for Grain Farming, Department of Arable Farming, Shortandy, 021601, Kazakhstan*
[g] *Department of Marine Sciences and Applied Biology, Multidisciplinary Institute for Environmental Studies "Ramón Margalef", University of Alicante, PO Box 99, Alicante, 03080, Spain*
[h] *Department of Botany and Plant Pathology, Oregon State University, Corvallis, OR, 97330, United States of America*
[i] *Division of Environmental Biology, National Science Foundation, Alexandria, VA, 22314, United States of America*
[j] *Plant-Microbe Interactions, Institute of Natural Resources and Agrobiology of Salamanca, IRNASA-CSIC, Salamanca, Spain*
[k] *Centre for Agricultural Research, Plant Protection Institute, Hungarian Research Network (HUN-REN), Herman Ottó u. 15, Budapest, 1022, Hungary*
[l] *Department of Pharmacognosy, Semmelweis University, Üllői út 26, Budapest, 1085, Hungary*

ARTICLE INFO

Keywords:
Darksidea
Lentitheciaceae
Endophytes
Specialized metabolites
Plant growth
Antibacterial activity

ABSTRACT

The endophytic fungal genus *Darksidea*, one of the most abundant members of root-associated fungal communities in Eurasian and North American grasslands, was investigated for its specialized metabolites. Molecular phylogenetic analysis of 51 *Darksidea* isolates revealed 15 well-supported clades, including eight potentially novel species. Following a metabolite screening of the *in vitro*-cultivated fungal isolates, 18 characteristic metabolites of the genus were identified and isolated. Their chemical structures were elucidated by high-performance liquid chromatography coupled with high-resolution tandem mass spectrometry (HPLC-HR-MS/MS), which revealed structure-specific fragmentation patterns. The structures were subsequently confirmed by nuclear magnetic resonance (NMR) spectroscopy. These analyses also led to the identification of four previously undescribed compounds: two eremophilane-type sesquiterpenes, 1-dehydroisopetasol and 3-petason, and two polyketides, mannuronyl-epicoccamide A and mannuronyl-epicoccamide D. Plant bioassay with *Lemna minor* showed that ten of the 18 compounds inhibited plant growth. In addition, the polyketide quinone ascomycone A exhibited mild antibacterial activity against both methicillin-resistant and methicillin-susceptible *Staphylococcus aureus strains*.

1. Introduction

Endophytic fungi colonize plant tissues internally and asymptomatically for extended periods during their life cycle (Porras-Alfaro and Bayman, 2011; Saikkonen et al., 1998). Root-colonizing endophytes, particularly dark septate endophytes (DSEs), are commonly found in healthy roots of grasses and are widespread in grassland ecosystems worldwide and frequent in abiotically stressed environments (Knapp

* Corresponding author. Department of Plant Anatomy, Institute of Biology, Eötvös Loránd University, Pázmány Péter sétány 1/C, Budapest, 1117, Hungary.
** Corresponding author. Department of Pharmacognosy, Semmelweis University, Üllői út 26, Budapest, 1085, Hungary.
E-mail addresses: gaborm.kovacs@ttk.elte.hu (G.M. Kovács), boldizsar.imre@semmelweis.hu (I. Boldizsár).
[1] Equally contributed.

https://doi.org/10.1016/j.phytochem.2026.115066
Received 30 December 2025; Received in revised form 18 August 2026; Accepted 20 August 2026
Available online 25 August 2026
0031-9422/© 2026 The Authors. Published by Elsevier Ltd. This is an open access article under the CC BY license (http://creativecommons.org/licenses/by/4.0/).

et al., 2012, 2019; Mandyam and Jumpponen, 2005; Porras-Alfaro et al., 2008). Many DSEs belong to the order *Pleosporales* (Knapp et al., 2012, 2015, 2019; Rodriguez et al., 2009; Sieber and Grünig, 2013), which accommodates numerous taxa rich in diverse specialized metabolites (Berek-Nagy et al., 2021; Maciá-Vicente et al., 2018; Nisa et al., 2015).

The specialized metabolites produced by endophytic fungi often play important ecological roles, especially in biotic interactions (Hardoim et al., 2015; Maciá-Vicente et al., 2018; Schulz et al., 2002). These compounds can protect host plants against a wide range of pathogenic, parasitic, and herbivorous organisms, including fungi (Li and Strobel, 2001), nematodes (Schwarz et al., 2004), and insects (Schardl et al., 2007). In addition, they may influence plant growth (Berthelot et al., 2016; Choi et al., 2004). Beyond their ecological functions, these metabolites can also have biomedical relevance, as they often exhibit diverse biological activities, including antibacterial effects (Deshmukh et al., 2022).

The genus *Darksidea* (*Lentitheciaceae, Pleosporales*) represents a dominant group of DSEs in grasslands across Europe, Asia, and North America (Knapp et al., 2012, 2015, 2019; Romero-Jiménez et al., 2022; Rudgers et al., 2022). Currently, seven species are recognized within this genus: *D. alpha*, *D. beta*, *D. gamma*, *D. delta*, *D. epsilon*, *D. phi*, and *D. zeta* (Knapp et al., 2015; Romero-Jiménez et al., 2022). However, analyses of additional sequence data from recent collections suggest the existence of further distinct lineages, potentially representing novel species within the genus (Romero-Jiménez et al., 2022). To date, no comprehensive study of specialized metabolites has been reported from *Darksidea* species. Given the widespread occurrence of specialized metabolites in other *Pleosporales* fungi and their ecological importance in endophytic lifestyles (Maciá-Vicente et al., 2018), it is reasonable to hypothesize that *Darksidea* species also produce a wide array of specialized metabolites.

The objectives of this study were therefore: (i) to isolate and identify characteristic specialized metabolites from *Darksidea* isolates representing different lineages and (ii) to assess the bioactivity of the isolated compounds, including plant growth-modulating and antibacterial effects.

2. Results and discussion

2.1. Molecular phylogenetic characterization of Darksidea isolates

A total of 51 *in vitro*-grown fungal isolates, identified as representatives of the endophytic fungal genus *Darksidea* based on molecular phylogenetic analyses of the nuclear ribosomal (nrDNA) internal transcribed spacer (ITS) region (Schoch et al., 2012), were included in this study (Supplementary Table S1). Among these isolates, four were newly introduced in this work through the determination of their nrDNA ITS sequences, while the remaining 47 had already been identified (Glynou et al., 2016; Knapp et al., 2015, 2019; Romero-Jiménez et al., 2022). Molecular phylogenetic analyses of all 51 *Darksidea* isolates revealed 15 distinct lineages (Fig. 1). Among these, seven clades corresponded to previously described *Darksidea* species (*D. alpha*, *D. beta*, *D. gamma*, *D. delta*, *D. epsilon*, *D. phi*, and *D. zeta*), while the remaining eight clades may represent novel taxa within the genus (Knapp et al., 2015; Romero-Jiménez et al., 2022) (Fig. 1).

2.2. Identification of compounds from in vitro cultures of Darksidea species

Metabolite screening of *in vitro* cultures of the 51 *Darksidea* isolates was performed using high-performance liquid chromatography (HPLC) coupled with ultraviolet (UV) spectrophotometry and high-resolution tandem mass spectrometry (HR-MS/MS). This analysis revealed 18 characteristic compounds, all of which were successfully isolated by preparative HPLC (Fig. 2, Supplementary Fig. S1). Extensive analysis of the mass fragment ion spectra of the isolated compounds, combined with their nuclear magnetic resonance (NMR) and circular dichroism (CD) spectroscopy analyses, enabled complete structure identifications (Figs. 3 and 4; Tables 1–3; Supplementary Figs. S2–S30; Tables S2–S7). The compounds were numbered according to their retention order as determined by the HPLC-UV-HR-MS/MS analysis (Supplementary Fig. S1).

To isolate all 18 target compounds with the fewest possible extraction and preparative HPLC separation steps, isolates of *D. alpha*, *D. beta*, *D. phi*, and the novel lineage "2" were selected based on their metabolite profiles, which together covered all characteristic compounds.

From the *in vitro* cultures of the species *D. alpha*, a total of ten compounds (**3**–**10**, **13**, and **14**) were identified and isolated. Among them, compounds **3**, **4**, and **6** share the same molecular formula, $C_{15}H_{22}O_2$, suggesting that they are isomers (Table 1). The UV absorption maxima of compound **4**, observed at 248 nm and 284 nm, show a bathochromic shift compared to those of compounds **3** and **6**, which absorb at around 240 nm (Supplementary Fig. S2). This shift suggests a more extended conjugated system in compound **4**. The UV spectral characteristics, together with the molecular formula $C_{15}H_{22}O_2$, are consistent with the structures of the eremophilane sesquiterpenes petasol (**3**), isopetasol (**4**), and 3-epi-petasol (**6**) (Fig. 2) (Le et al., 2013; Sugama et al., 1983). Due to the presence of four chiral centers at C-3, C-4, C-5, and C-7 in petasol and 3-epi-petasol, and three chiral centers at C-3, C-4, and C-5 in isopetasol, unambiguous structural identification required complementary NMR and CD spectroscopic analyses together with optical rotation measurements. These analyses identified the compounds as 3*R*,4*R*,5*R*,7*S*-petasol, 3*R*,4*R*,5*R*-isopetasol, and 3*S*,4*R*,5*R*,7*S*-epi-petasol (see details in the Supplementary Material, page S6; Figs. S3, S4, S28, Table S2) (Daengrot et al., 2015; Le et al., 2013; Sugama et al., 1983; Wang et al., 2014).

Compounds **5** and **7** can be identified by their identical molecular formula, $C_{15}H_{20}O_2$, which has two fewer hydrogens than that of petasol and its isomers (**3**, **4**, and **6**) (Table 1). The characteristic fragment ions generated from the protonated molecules of compounds **5** and **7** (*m/z* 233, $C_{15}H_{21}O_2$) are the same: Both compounds exhibit fragment ions at *m/z* 215.14 ($C_{15}H_{19}O$), *m/z* 205.16 ($C_{14}H_{21}O$), *m/z* 197.13 ($C_{15}H_{17}$), and *m/z* 187.15 ($C_{14}H_{19}$) (Supplementary Fig. S4). These ions appear to be generated via the same fragmentation pathways as the corresponding fragment ions observed for the petasol isomers (**3**, **4**, and **6**; see Supplementary Material, page S6). Specifically, they arise by the loss of one (*m/z* 215.14, $C_{15}H_{19}O$) or two water molecules (*m/z* 197.13, $C_{15}H_{17}$), by the loss of a carbon monoxide molecule (*m/z* 205.16, $C_{14}H_{21}O$), or by the consecutive loss of both CO and H_2O (*m/z* 187.15, $C_{14}H_{19}$). Comparison of these fragment ions with those obtained from petasol and its isomers shows that compounds **5** and **7** are closely related to these structures. In addition, each fragment ion contains two fewer hydrogen atoms than the corresponding ions of the petasol isomers (**3**, **4**, and **6**) (Supplementary Fig. S4). The mass spectral data indicate a close structural relationship between the petasol isomers and compounds **5** and **7**, suggesting that compounds **5** and **7** are oxidized derivatives of the petasol isomers. The fragment ion at *m/z* 205.16 ($C_{14}H_{21}O$) can be generated by the elimination of the carbonyl group as carbon monoxide from the protonated compounds **5** and **7**. The markedly lower intensity of the fragment ion at *m/z* 205.16 in the mass spectrum of compound **5**, relative to that of compound **7**, suggests that the carbonyl group in compound **5** is involved in an extended conjugated system (Supplementary Fig. S4). Such conjugation likely contributes to the enhanced stabilization of compound **5**, as also observed for compound **4** (see Supplementary Material, page S6). The bathochromic shift in the UV spectrum of compound **5**, compared to that of compound **7**, provides additional evidence for a more extended conjugated system in compound **5** (Supplementary Fig. S2).

Unequivocal structural elucidation of compounds **5** and **7** was achieved by NMR spectroscopy (Table 2, Supplementary Figs. S5 and S6). Comparing the ^{1}H NMR spectra of the petasol isomers **3**, **4**, and **6** with that of compound **5** (Supplementary Figs. S3 and S5), the most

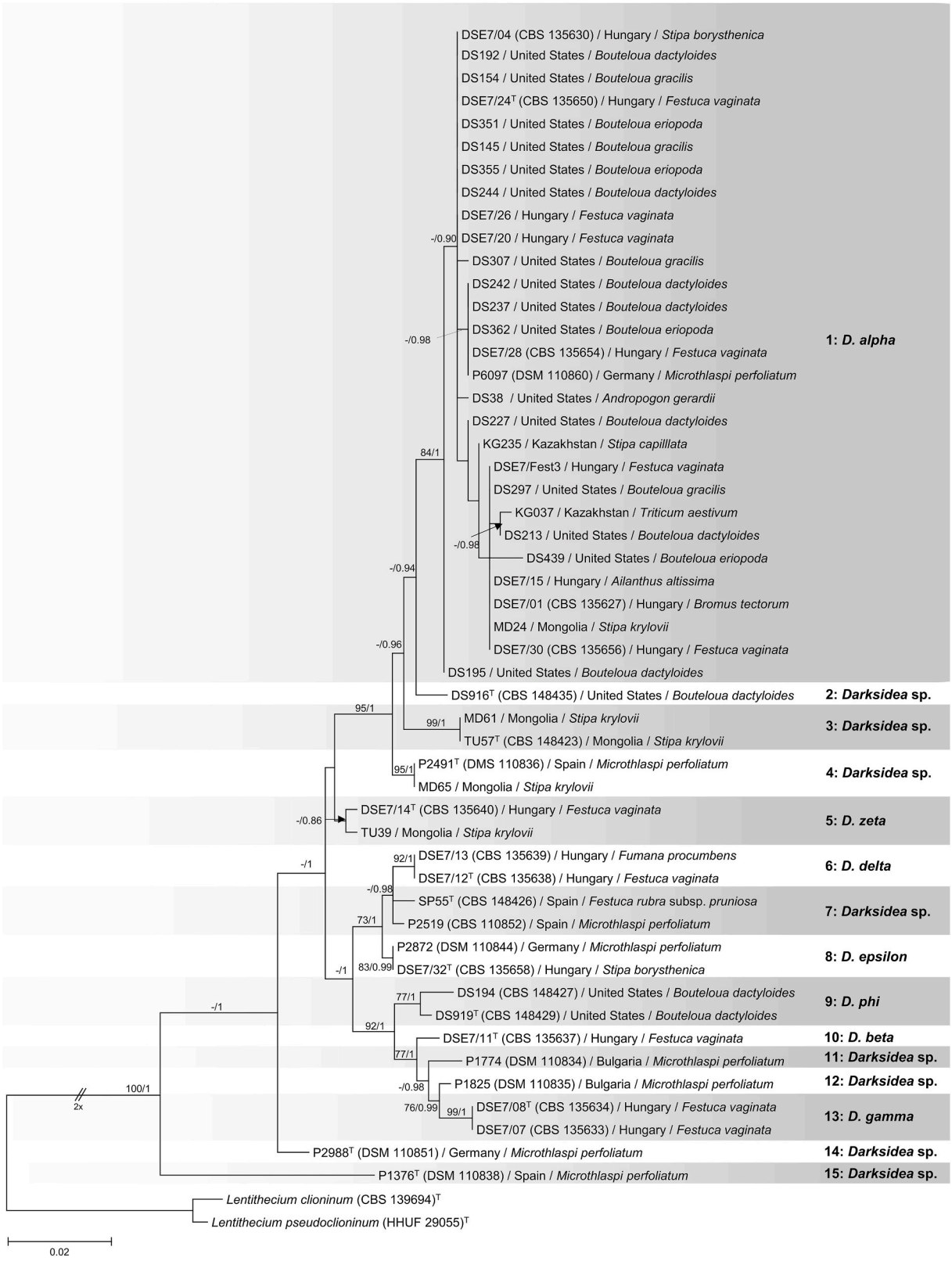

Fig. 1. Phylogenetic tree of the 51 *Darksidea* isolates analyzed. The tree was inferred using sequences of the nuclear ribosomal internal transcribed spacer (nrDNA ITS) region via Maximum Likelihood (ML) and Bayesian Inference methods. ML bootstrap support values (≥70) and Bayesian posterior probabilities (≥0.90) are indicated at the nodes, before and after the slashes, respectively. Potentially novel lineages are labeled as *Darksidea* sp. Isolate and culture collection numbers, countries of origin, and host plant species are also indicated. Type materials are indexed with letter T. *Lentithecium clioninum* (CBS 139694) and *L. pseudoclioninum* (HHUF 29055) were used as outgroup taxa. The scale bar indicates 0.02 expected changes per site per branch.

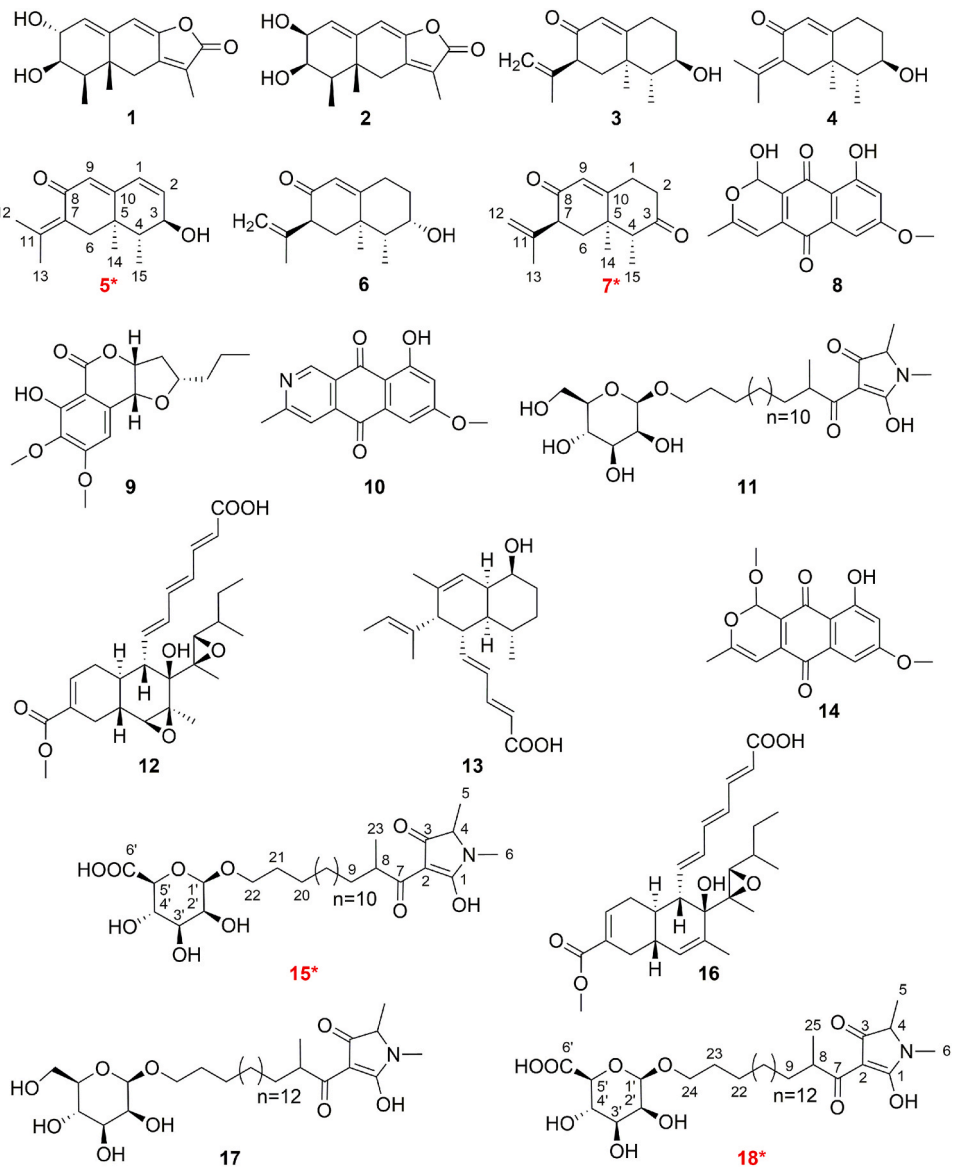

Fig. 2. Structures of compounds (**1**–**18**) identified from *in vitro* cultures of *Darksidea* species. Previously undescribed compounds are marked in red and indicated with an asterisk.

prominent difference is the appearance of a proton signal at 6.14 ppm with an integral value of two in the case of compound **5**. This observation indicates the presence of an additional conjugated carbon-carbon double bond in the structure of compound **5**. The absence of the two characteristic vinyl proton signals around 5 ppm suggests that compound **5** is a derivative of isopetasol (compound **4**). This interpretation is further supported by the presence of four methyl proton signals (H-12, H-13, H-14, and H-15) at chemical shifts very similar to those observed in the ^{1}H NMR spectrum of isopetasol. In the HMBC spectrum of compound **5**, the 6.14 ppm proton signal shows correlations with two sp^{2} hybridized carbon atoms at 159.2 ppm (C-10) and 127.3 ppm (C-9), a hydroxylated carbon at 71.4 ppm (C-3), and two aliphatic carbon atoms at 47.3 ppm (C-4) and 39.5 ppm (C-5) (Supplementary Fig. S5). These correlations confirm that the additional double bond is located between the C-1 and C-2 carbon atoms of the isopetasol framework, thereby extending the conjugated double bond system of the molecule.

The ^{1}H NMR spectrum of compound **7** in $CDCl_3$ closely resembles that of petasol (compound **3**) recorded in the same solvent (Table 2, Supplementary Figs. S3, S6, Table S2), with the notable exception of the absence of the H-3 proton signal at 3.62 ppm. Additionally, the H-1, H-2, and H-4 signals are shifted downfield. Consistent with these changes, the ^{13}C NMR spectrum of compound **7** shows the appearance of a new carbonyl carbon signal at 209.8 ppm, replacing the aliphatic oxygenated sp^{3} carbon signal observed around 70 ppm in petasol. This shift confirms the oxidation of the secondary alcohol at C-3 to a ketone. HMBC correlations between the carbonyl carbon and both the H-15 methyl signal at 1.06 ppm and the multiplet signals between 2.50 and 2.62 ppm and at 2.76 ppm (assigned to H-2, H-4, and H-1) further support this structural modification.

These findings support the identification of compounds **5** and **7** as previously undescribed natural eremophilane sesquiterpenes, designated as 1-dehydroisopetasol and 3-petason, respectively (Fig. 2).

The positive signal observed at 230–260 nm in the CD spectrum of compound **5** corresponds to the π → π* transition of the enone chromophore. This feature can be interpreted using the cyclohexanone chirality (helicity) rule, which correlates the three-dimensional structure of the molecule with the sign of the CD signal (Supplementary Fig. S28). When the molecule is viewed from the C═C double bond toward the C═O group, a clockwise (right-handed) twist results in a positive Cotton effect. In this stereochemical arrangement, the enone

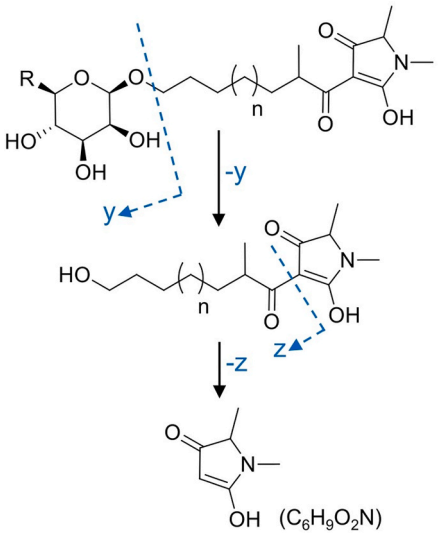

Fig. 3. Proposed fragmentation pathways of epicoccamide A (**11**, R = –CH_2OH, n = 10), epicoccamide D (**17**, R = –CH_2OH, n = 12), mannuronyl-epicoccamide A (**15**, R = –COOH, n = 10), and mannuronyl-epicoccamide D (**18**, R = –COOH, n = 12). The eliminated structural units, labeled as y and z, correspond to the y and z fragments shown in Fig. 4.

system adopts a right-handed twist (positive helicity) to minimize unfavorable methyl–methyl interactions. Because the scaffold enforces a positive (P) helicity, the π → π* transition is expected to produce a positive CD signal. The positive signal around 235 nm in the CD spectrum of compound **7** can likewise be explained by the helicity rule, whereas the spectral region around 290 nm is governed by the octant rule, leading to a negative Cotton effect. These results indicate that the configurations of the corresponding chiral centers in compounds **5** and **7** are identical to those in compounds **3** and **4** (Supplementary Fig. S28).

The 3*R*,4*R*,5*R* configuration of 1-dehydroisopetasol was further supported by computational analysis. The calculated CD spectra of 3*R*,4*R*,5*R*-1-dehydroisopetasol and its 3*S*,4*S*,5*S* enantiomer exhibited the expected mirror-image relationship (Supplementary Fig. S28). The experimental CD spectrum of compound **5** agreed well with the calculated spectrum of the 3*R*,4*R*,5*R* enantiomer, except for an approximately 25 nm blue shift in the calculated spectrum, confirming compound **5** as 3*R*,4*R*,5*R*-1-dehydroisopetasol. In contrast, comparison of the calculated and experimental CD spectra of compound **7** was inconclusive. Nevertheless, considering the interpretation of its CD spectrum and the most plausible biosynthetic pathways involving enzymatic oxidation of 3R,4R,5R-isopetasol and 3R,4R,5R,7S-petasol to yield compounds **5** and **7**, respectively, the same configuration at the corresponding stereocenters in compound **7** appears likely. Accordingly, compound **7** is proposed to be 4*R*,5*R*-3-petason.

Four compounds (**11**, **15**, **17**, **18**) were isolated from *in vitro* cultures of *D. beta*. They exhibited comparable UV spectra, each showing an absorption maximum at approximately 280 nm (Supplementary Fig. S2). Interpretation of the UV spectral data, together with the molecular formulas determined by HR-MS (compound **11**: $C_{29}H_{51}O_9N$; compound **17**: $C_{31}H_{55}O_9N$ and the characteristic fragment ions observed in their HR-MS/MS spectra (indicative of hexosyl loss and a substituted tetramic acid moiety) allowed the tentative identification of compounds **11** and **17** as mannose-containing glycosidic tetramic acid derivatives (see details in the Supplementary Material, page S9; Figs. S16, S17, Table 1, Figs. 3 and 4). Thus, compound **11** was identified as epicoccamide A (Wright et al., 2003), while compound **17** was assigned as epicoccamide D, a close structural analogue featuring an aliphatic chain extended by two methylene units (Wangun et al., 2007) (Fig. 2).

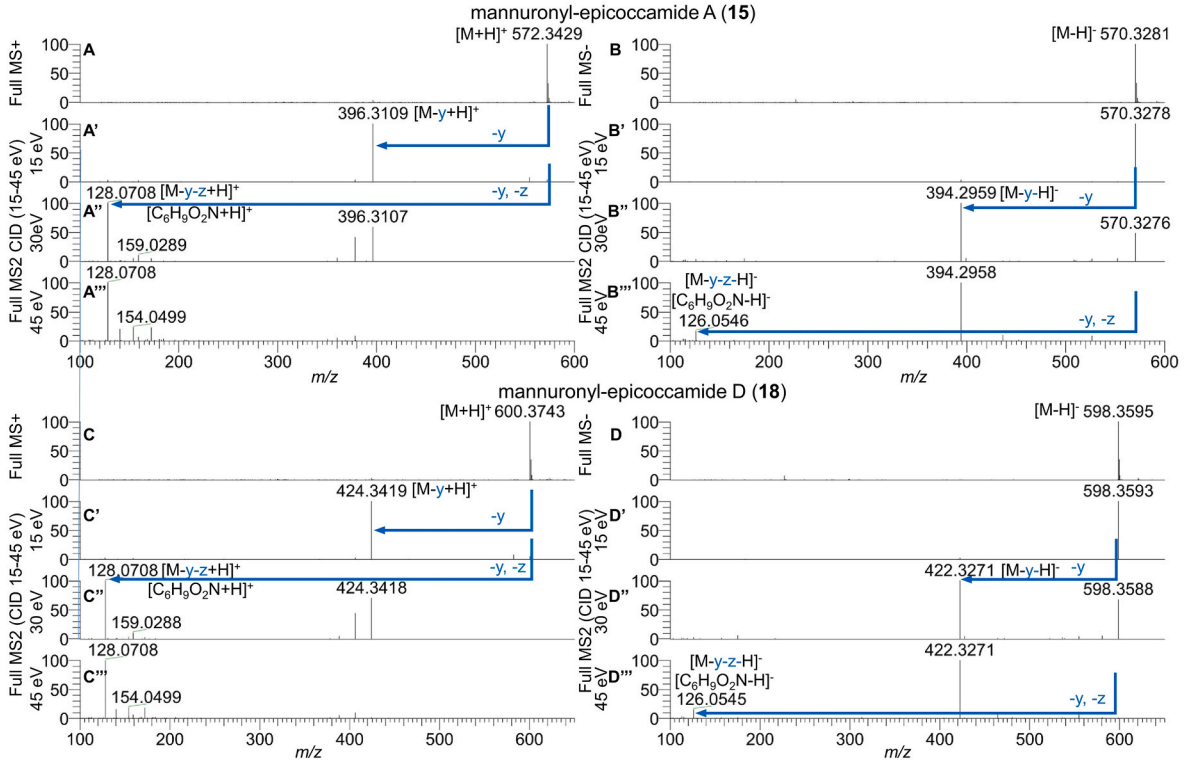

Fig. 4. Mass spectra (A, B, C, D) and tandem mass spectra (A′–A‴, B′–B‴, C′–C‴, D′–D‴) of mannuronyl-epicoccamide A (**15**) (A, A′–A‴, B, B′–B‴) and mannuronyl-epicoccamide D (**18**) (C, C′–C‴, D, D′–D‴) acquired in positive (A, A′–A‴, C, C′–C‴) and negative (B, B′–B‴, D, D′–D‴) ionization modes. Tandem mass spectra of compounds **15** and **18** were generated from their protonated molecules at *m/z* 572 and *m/z* 600 (positive mode) and from their deprotonated molecules at *m/z* 570 and *m/z* 598 (negative mode), respectively, using collision-induced dissociation (CID) at 15 eV (A′, B′, C′, D′), 30 eV (A″, B″, C″, D″), and 45 eV (A‴, B‴, C‴, D‴). The proposed structures of the eliminated fragments labeled y and z are shown in Fig. 3, using the same symbols (*y* and *z*).

Table 1
High-resolution mass spectral data for compounds identified in *Darksidea* culture extracts.

compound			detected ion	detected formula	detected *m/z*	diff (ppm)
No.	name	formula				
1	2-epi-PF1092C	$C_{15}H_{18}O_4$	$[M+H]^+$	$C_{15}H_{19}O_4$	263.1274	−1.427
			$[M+Na]^+$	$C_{15}H_{18}O_4Na$	285.1090	−2.456
			$[M+NH_4]^+$	$C_{15}H_{22}O_4N$	280.1541	−1.016
			$[M-H]^-$	$C_{15}H_{17}O_4$	261.1131	−0.392
			$[M+COOH]^-$	$C_{16}H_{19}O_6$	307.1188	+0.418
2	PF1092C	$C_{15}H_{18}O_4$	$[M+H]^+$	$C_{15}H_{19}O_4$	263.1273	−1.655
			$[M+Na]^+$	$C_{15}H_{18}O_4Na$	285.1091	−2.316
			$[M+NH_4]^+$	$C_{15}H_{22}O_4N$	280.1541	−0.802
			$[M-H]^-$	$C_{15}H_{17}O_4$	261.1133	+0.183
			$[M+COOH]^-$	$C_{16}H_{19}O_6$	307.1189	+0.516
3	petasol	$C_{15}H_{22}O_2$	$[M+H]^+$	$C_{15}H_{23}O_2$	235.1689	−1.601
			$[M+Na]^+$	$C_{15}H_{22}O_2Na$	257.1509	−1.132
4	isopetasol	$C_{15}H_{22}O_2$	$[M+H]^+$	$C_{15}H_{23}O_2$	235.1688	−1.984
			$[M+Na]^+$	$C_{15}H_{22}O_2Na$	257.1512	+0.034
5	1-dehydro-isopetasol	$C_{15}H_{20}O_2$	$[M+H]^+$	$C_{15}H_{21}O_2$	233.1533	−1.357
			$[M+Na]^+$	$C_{15}H_{20}O_2Na$	255.1346	−3.571
6	3-epi-petasol	$C_{15}H_{22}O_2$	$[M+H]^+$	$C_{15}H_{23}O_2$	235.1683	−3.940
			$[M+Na]^+$	$C_{15}H_{22}O_2Na$	257.1502	−3.738
7	3-petason	$C_{15}H_{20}O_2$	$[M+H]^+$	$C_{15}H_{21}O_2$	233.1527	−3.759
			$[M+COOH]^-$	$C_{16}H_{21}O_4$	277.1442	−1.199
8	ascomycone B	$C_{15}H_{12}O_6$	$[M+H]^+$	$C_{15}H_{13}O_6$	289.0701	−1.849
			$[M+Na]^+$	$C_{15}H_{12}O_6Na$	311.0521	−1.766
			$[M-H]^-$	$C_{15}H_{11}O_6$	287.0562	+0.135
9	monocerin	$C_{16}H_{20}O_6$	$[M+H]^+$	$C_{16}H_{21}O_6$	309.1326	−1.859
			$[M+Na]^+$	$C_{16}H_{20}O_6Na$	331.1146	−1.962
10	6-deoxy-bostrycoidin	$C_{15}H_{11}O_4N$	$[M+H]^+$	$C_{15}H_{12}O_4N$	270.0756	−1.719
			$[M-H]^-$	$C_{15}H_{10}O_4N$	268.0616	+0.182
11	epicoccamide A	$C_{29}H_{51}O_9N$	$[M+H]^+$	$C_{29}H_{52}O_9N$	558.3630	−1.108
			$[M+Na]^+$	$C_{29}H_{51}O_9NNa$	580.3448	−1.401
			$[M+NH_4]^+$	$C_{29}H_{55}O_9N_2$	575.3887	−2.568
			$[M-H]^-$	$C_{29}H_{50}O_9N$	556.3493	+0.350
12	F2928-1	$C_{27}H_{36}O_7$	$[M+H]^+$	$C_{27}H_{37}O_7$	473.2529	−1.014
			$[M+Na]^+$	$C_{27}H_{36}O_7Na$	495.2346	−1.423
			$[M+NH_4]^+$	$C_{27}H_{40}O_7N$	490.2793	−1.222
			$[M-H]^-$	$C_{27}H_{35}O_7$	471.2387	−0.184
			$[M+COOH]^-$	$C_{28}H_{37}O_9$	517.2443	+0.027
13	phomopsidin	$C_{21}H_{30}O_3$	$[M+H]^+$	$C_{21}H_{31}O_3$	331.2262	−1.634
			$[M+Na]^+$	$C_{21}H_{30}O_3Na$	353.2081	−1.744
			$[M+NH_4]^+$	$C_{21}H_{34}O_3N$	348.2527	−1.724
			$[M-H]^-$	$C_{21}H_{29}O_3$	329.2124	+0.461
			$[M+COOH]^-$	$C_{22}H_{31}O_5$	375.2178	+0.354
14	ascomycone A	$C_{16}H_{14}O_6$	$[M-H]^-$	$C_{16}H_{13}O_6$	301.0717	−0.038
15	mannuronyl-epicoccamide A	$C_{29}H_{49}O_{10}N$	$[M+H]^+$	$C_{29}H_{50}O_{10}N$	572.3424	−0.896
			$[M+Na]^+$	$C_{29}H_{49}O_{10}NNa$	594.3240	−1.393
			$[M-H]^-$	$C_{29}H_{48}O_{10}N$	570.3286	+0.316
16	F2928-2	$C_{27}H_{36}O_6$	$[M+H]^+$	$C_{27}H_{37}O_6$	457.2579	−1.302
			$[M+Na]^+$	$C_{27}H_{36}O_6Na$	479.2399	−1.002
			$[M+NH_4]^+$	$C_{27}H_{40}O_6N$	474.2846	−0.916
			$[M-H]^-$	$C_{27}H_{35}O_6$	455.2440	+0.171
			$[M+COOH]^-$	$C_{28}H_{37}O_8$	501.2496	+0.416
17	epicoccamide D	$C_{31}H_{55}O_9N$	$[M+H]^+$	$C_{31}H_{56}O_9N$	586.3940	−1.567
			$[M+Na]^+$	$C_{31}H_{55}O_9NNa$	608.3757	−1.929
			$[M+NH_4]^+$	$C_{31}H_{59}O_9N_2$	603.4214	−0.261
			$[M-H]^-$	$C_{31}H_{54}O_9N$	584.3806	+0.367
18	mannuronyl-epicoccamide D	$C_{31}H_{53}O_{10}N$	$[M+H]^+$	$C_{31}H_{54}O_{10}N$	600.3732	−1.654
			$[M+Na]^+$	$C_{31}H_{53}O_{10}NNa$	622.3550	−1.812
			$[M+NH_4]^+$	$C_{31}H_{57}O_{10}N_2$	617.3997	−1.802
			$[M-H]^-$	$C_{31}H_{52}O_{10}N$	598.3599	+0.418

The HR-MS spectra of compound **15**, obtained in both positive and negative ionization modes, showed protonated and deprotonated ions at *m/z* 572.34 ($C_{29}H_{50}O_{10}N$) and *m/z* 570.33 ($C_{29}H_{48}O_{10}N$), respectively (Fig. 4, Table 1). The HR-MS/MS spectra of these ions revealed fragment ions at *m/z* 396.31 ($C_{23}H_{42}O_4N$) and at *m/z* 394.30 ($C_{23}H_{40}O_4N$), confirming that compound **15** contains the same aglycone unit as epicoccamide A (**11**) (Figs. 2–4). Further evidence for the shared aglycone unit between compounds **15** and **11** was obtained from the detection of ions at *m/z* 128.07 ($C_6H_{10}O_2N$) and *m/z* 126.05 ($C_6H_8O_2N$) in the HR-MS/MS spectra of compound **15**, recorded in the positive and negative ionization modes, respectively. These correspond to the protonated and deprotonated forms of the substituted tetramic acid unit, also observed in the HR-MS/MS spectra of epicoccamide A (Figs. 3 and 4, Supplementary Fig. S16). The difference between the molecular formulas of protonated compound **15** and its fragment ion ($C_{29}H_{50}O_{10}N$ vs. $C_{23}H_{42}O_4N$), as well as between the deprotonated forms ($C_{29}H_{48}O_{10}N$ vs $C_{23}H_{40}O_4N$), corresponds to $C_6H_8O_6$. This difference indicates the presence of a hexuronic acid moiety in compound **15**, which can be cleaved during fragmentation under both ionization modes (Figs. 3 and 4). Based on these analytical results, compound **15** was tentatively identified as a hexuronic acid-containing analogue of epicoccamide A. The protonated and deprotonated molecules of compound **18**, detected at *m/z* 600.37 ($C_{31}H_{54}O_{10}N$) and *m/z* 598.36 ($C_{31}H_{52}O_{10}N$), were both found to lose a hexuronic acid unit during fragmentation. This was

Table 2
^{1}H and ^{13}C NMR data for compounds **5** and **7** in $CDCl_3$ (δ in ppm, J in Hz).

No.	5		7	
	δ_H	δ_C	δ_H	δ_C
1	6.14 (m, overl.)	128.1	2.76 (m)	32.1
2	6.14 (m, overl.)	139.4	2.56 (m overl.)	40.0
3	4.05 (t, 8.6)	71.4	-	209.8
4	1.59 (m)	47.3	2.52 (m, overl.)	54.1
5	-	39.5	-	43.2
6	2.93 (d, 14.3) 2.18 (m)	39.8	2.09 (t, 13.6) 2.01 (dd, 13.1, 4.8)	41.6
7	-	127.2	3.11 (dd, 14.1, 4.8)	50.8
8	-	191.5	-	198.3
9	5.78 (s)	127.3	5.93 (s)	125.5
10	-	159.2	-	164.3
11	-	146.1	-	143.1
12	2.17 (s)	23.4	5.02 (br s) 4.84 (br s)	114.9
13	1.89 (s)	23.0	1.76 (s)	20.3
14	0.95 (s)	16.6	1.14 (s)	18.1
15	1.16 (d, 6.7)	10.5	1.06 (d, 6.7)	7.3

Table 3
^{1}H and ^{13}C NMR data for compounds **15** and **18** in CD_3OD (δ in ppm, J in Hz).

No.	15		18	
	δ_H	δ_C	δ_H	δ_C
1	-	173.4[a]	-	173.8[a]
2	-	101.9	-	ND
3	-	197.9[a]	-	198.1[a]
4	3.80 m (overl.)	63.5	3.76 br q (overl.)	63.4[a]
5	1.33 d (7.0)	15.3	1.32 d (7.1)	15.4
6	2.95 s	26.7	2.94 s	26.7
7		193.9[a]	-	ND
8	3.65 br q (6.9)	37.6	3.67 br m (overl.)	38.1[a]
9	1.69 m 1.45 m	35.0	1.69 m 1.45 m (overl.)	35.0
10	1.29 m	28.5	1.28 m (overl.)	28.6
11-19(21)	1.25-1.40 m	30.7-31.0	1.25-1.40 m	30.7-31.0
20	1.37 m	27.3	-	-
21	1.61 m	30.9	-	-
22	3.88 td (6.7, 9.5) 3.54 m	71.1	1.36 m	27.3
23	1.15 d (6.9)	17.7	1.61 m	30.9
24	-		3.90 m 3.54 m	71.1
25	-		1.12 d (6.9)	17.8
1′	4.57 d (0.7)	102.3	4.56 d (0.7)	102.2
2′	3.86 dd (3.2, 0.7)	72.4	3.86 dd (3.3, 0.7)	72.4
3′	3.48 dd (9.3, 3.2)	74.9	3.48 dd (9.3, 3.3)	75.0
4′	3.81 t (9.5)	70.1	3.80 t (9.5)	70.2
5′	3.70 d (9.7)	77.3	3.68 d (9.7)	77.3
6′	-	173.2	-	173.8[a]

[a] from HMBC.

evidenced by the observation of fragment ions at *m/z* 424.34 ($C_{25}H_{46}O_4N$) and *m/z* 422.33 ($C_{25}H_{44}O_4N$) in the corresponding HR-MS/MS spectra (Figs. 3 and 4). The mass differences between the precursor and fragment ions (*m/z* 600.37 to 424.34 and *m/z* 598.36 to 422.33) correspond to $C_6H_8O_6$, confirming the loss of a hexuronic acid moiety. These fragment ions at *m/z* 424.34 and 422.33, representing the aglycone part of compound **18**, are identical to those observed for the aglycone part of epicoccamide D (compound **17**) (Supplementary Fig. S17). Moreover, the HR-MS/MS spectra of compound **18** also showed ions at *m/z* 128.07 ($C_6H_{10}O_2N$) and *m/z* 126.05 ($C_6H_8O_2N$), corresponding to the substituted tetramic acid unit present in compounds **11**, **15**, and **17**, detected in the positive and negative ionization modes, respectively (Figs. 3 and 4, Supplementary Figs. S16, S17). These findings support the tentative identification of compound **18** as a hexuronic acid-containing analogue of epicoccamide D. Assuming a similar biosynthetic pathway for compounds **11**, **15**, **17**, and **18**, we propose that compounds **15** and **18** represent previously undescribed natural analogues of epicoccamide A and epicoccamide D. In these compounds, the mannose moiety is replaced by mannuronic acid. The structures of these two previously undescribed compounds, designated as mannuronyl-epicoccamide A (**15**) and mannuronyl-epicoccamide D (**18**), were further confirmed through comprehensive NMR analyses. Initially, the ^{1}H NMR spectra of the parent compounds epicoccamides A and D (compounds **11** and **17**) were recorded in methanol-d_4 (Supplementary Table S4, Figs. S18, S19) and compared with previously published data (Wangun et al., 2007; Wright et al., 2003), showing excellent agreement. Subsequently, 1D (^{1}H and ^{13}C) and 2D homonuclear and heteronuclear correlation NMR experiments were performed on the methanol solution of compounds **15** and **18** (Table 3, Supplementary Figs. S20, S21). The aglycone moieties of compounds **15** and **18** exhibited nearly identical chemical shift values and coupling patterns to those of their respective parent compounds **11** and **17**, confirming structural consistency. In contrast, notable differences were observed in the sugar moieties. The most significant change was a downfield shift of approximately 0.5 ppm in the H-5′ protons, accompanied by a simplification of their splitting pattern from a doublet-doublet-doublet in the parent compounds to a simple doublet in the derivatives. Additionally, the H-6 proton signals were absent, suggesting oxidation at the C-6 position. Supporting this interpretation, HMBC cross-peak was detected between H-5' at 3.70 and 3.68 ppm in compounds **15** and **18**, and carbonyl carbons at 173.2 and 173.8 ppm, respectively.

These findings confirm that compounds **15** and **18** correspond to mannuronyl-epicoccamide A and mannuronyl-epicoccamide D, respectively, and represent two previously undescribed natural metabolites (Fig. 2). Nevertheless, not all carbon signals could be observed in the $1D^{13}C$ NMR spectra of these mannuronic acid derivatives. Certain quaternary carbon atoms (particularly carbonyl carbons) were only detectable in the more sensitive inverse-detected HMBC experiments.

Based on the literature, the configurations of the chiral carbons C4 and C8 in the known compounds **11** and **17** could not be determined using derivatization- or CD measurement-based techniques (Wangun et al., 2007; Wright et al., 2003). Considering the apparent difficulty in determining the conformations at positions C4 and C8, we aimed to determine the absolute configuration of the mannuronic acid unit in the previously undescribed compounds **15** and **18**. Acid hydrolysis of compound **11** from *D. alpha* resulted in the formation of an aglycone unit and a sugar unit. These were identified by HPLC-HR-MS, which indicated a molecular formula of $C_{23}H_{41}O_4N$ for the aglycone, and by polarimetry, which gave [α] +16.1 (*c* 0.1, H_2O) for the sugar unit (Supplementary Fig. S29). These results further support the proposed structure of compound **11** by identifying its aglycone moiety. Moreover, they confirm the D configuration of its β-mannose unit (Wright et al., 2003). However, because acidic hydrolysis conditions may induce lactonization of mannuronic acid, accompanied by changes in its optical rotation, the absolute configuration of the mannuronic acid-containing compounds **15** and **18** could not be determined using an optical rotation-based method after acid hydrolysis (Schoeffel and Link, 1933). Nevertheless, considering the common biosynthetic pathway in which mannuronic acid is formed from mannose via enzymatic oxidation, it is highly likely that the mannuronic acid unit in compounds **15** and **18** possesses the same absolute configuration as mannose (Tenhaken et al., 2011). Based on biosynthetic considerations, the mannuronic acid moiety is likely to possess the D configuration. Although the configurations at C4 and C8 could not be definitively determined, the CD spectra of the four epicoccamides are highly similar, exhibiting peak maxima and minima consistent with the reported CD data for epicoccamide A (Supplementary Fig. S29) (Wright et al., 2003). This observation suggests that the absolute configurations at the chiral centers C4 and C8 are conserved among these compounds from *D. beta* and epicoccamide A reported in the literature (Wright et al., 2003).

The structurally complex compounds epicoccamide A and D,

members of the polyketide-nonribosomal peptide hybrid class, had previously been reported only from the fungal genera *Epicoccum* and *Phomopsis* (Gakuubi et al., 2022; Wangun et al., 2007), underscoring the significance of *D. beta* as a new natural source of these rare metabolites.

Among the eremophilane sesquiterpenes (compounds **3**–**7**) identified in *D. alpha*, compounds **3** and **4** are known to be produced by both fungi and plants. They have been reported to co-occur in certain natural sources, such as the plant *Petasites pyrenaicus* (*P. fragrans*) (Sugama et al., 1983) and the soil fungus *Penicillium copticola* (Daengrot et al., 2015). In contrast, compound **6** has only been reported from a mycobiont of the lichen *Sarcographa tricosa* (Le et al., 2013).

Three colored compounds, either red (**8**, **14**) or yellow (**10**), were also isolated from the *in vitro* cultures of *D. alpha*, exhibiting UV absorption maxima at 278, 350, and 488 nm (**8**, **14**) and at 240, 272, and 416 nm (**10**) (Supplementary Fig. S2). Based on their molecular formulas determined by HR-MS analysis and their characteristic UV spectra, compounds **8** and **14** were tentatively identified as the polyketide-type pyranonaphthoquinones ascomycone B ($C_{15}H_{12}O_6$) and ascomycone A ($C_{16}H_{14}O_6$), respectively, while compound **10** was tentatively assigned as a related polyketide, the 2-aza-anthraquinone derivative 6-deoxybostrycoidin ($C_{15}H_{11}O_4N$) (Opatz et al., 2008; Parisot et al., 1989) (Table 1, Fig. 2).

The closely related fungal metabolites **8**, **10**, and **14** commonly co-occur in their natural sources, most likely as a result of a fungal detoxification mechanism in which pyranonaphthoquinones react with excess ammonia to form their 2-aza-anthraquinone counterparts (Jacobs et al., 2011; Stodůlková et al., 2015; Xie et al., 2020).

Compounds **9** and **13** were also isolated from *in vitro* cultures of *D. alpha*, characterized by the molecular formulas of $C_{16}H_{20}O_6$ and $C_{21}H_{30}O_3$ and UV absorption maximum at 274 nm and 268 nm, respectively (Table 1, Supplementary Fig. S2). Based on these data, two further polyketides, monocerin (**9**) and phomopsidin (**13**), were presumed to be produced by *D. alpha* (Fig. 2) (Aldridge and Turner, 1970; Kobayashi et al., 2003).

The identities of the polyketides (**8**, **9**, **10**, **13**, and **14**) were further confirmed by structure-specific fragment ions obtained from HR-MS/MS analyses (see details in the Supplementary Material, page S8; Figs. S7–S10) and by their NMR spectroscopic data, which closely matched previously reported values in the literature (Supplementary Figs. S11–S15, Table S3) (Namikoshi et al., 1997; Opatz et al., 2008; Parisot et al., 1989; Sappapan et al., 2008).

In addition to producing two previously undescribed eremophilane sesquiterpenes (1-dehydroisopetasol and 3-petason), one extremely rare compound (3-epi-petasol), and two common ones (petasol and isopetasol), cultures of *D. alpha* also yielded five relatively common polyketides (**8**, **9**, **10**, **13**, and **14**). Together, these findings demonstrate for the first time that this endophytic fungus is a rich source of specialized metabolites.

Compounds **1** and **2** were isolated from *in vitro* cultures of *Darksidea* clade 2. The HPLC-UV-HR-MS analysis revealed similar UV spectra, with absorption maxima between 322 and 326 nm, and identical molecular formulas ($C_{15}H_{18}O_4$) for both compounds (Table 1, Supplementary Fig. S2). These results, together with the identical fragment ions observed in the HR-MS/MS spectra of compounds **1** and **2** in positive ionization mode (see details in the Supplementary Material, page S10), suggest that the two compounds are isomers. Based on these findings and NMR spectral data comparable to those reported in the literature (Cheng et al., 2016; Tabata et al., 1997), compounds **2** and **1** were identified as PF1092C and its C-2 epimer (2-epi-PF1092C), respectively (Fig. 2, Supplementary Table S5, Figs. S22, S23, S24).

Compounds **1** and **2** have been identified in only one and two fungal species, respectively. Notably, only the *in vitro* culture of *Darksidea* clade 2 produces both compounds, providing a single source for their isolation (Cheng et al., 2016; Qin et al., 2015; Tabata et al., 1997).

Two compounds, **12** and **16**, were isolated from the *in vitro* cultures of *D. phi*. The UV spectra of these compounds were identical, showing an absorption maximum at 303 nm, while their molecular formulas, $C_{27}H_{36}O_7$ (**12**) and $C_{27}H_{36}O_6$ (**16**), differed by only one oxygen atom, suggesting highly similar structures (Table 1, Supplementary Fig. S2). Based on these analytical results, supported by the identification of structure-specific fragment ions in the HR-MS/MS spectra obtained in positive ionization mode (see details in the Supplementary Material, page S10; Fig. S25), the polyketides F2928-1 (**12**) and F2928-2 (syn cladobotric acid E, **16**) were tentatively identified in the cultures of *D. phi* (Fig. 2) (Kanai et al., 2005; Mitova et al., 2006).

NMR analysis also confirmed the identities of compounds **12** and **16** as F2928-1 and F2928-2, respectively, based on their spectroscopic data, which closely matched those reported in the literature (Supplementary Table S6, Figs. S26, S27) (Kanai et al., 2005).

Given that the extremely rare compounds **12** and **16** have been identified in only one and two fungal species, respectively, confirming *D. phi* as a new natural source of these compounds is particularly significant for isolation purposes (Kanai et al., 2005; Mitova et al., 2006).

2.3. Chemotaxonomic relevance of the identified compounds

Comparison of the identified compounds across the 51 fungal isolates representing 15 lineages (Fig. 1) revealed correlations between metabolite profiles and taxonomy. Most importantly, all isolates of all species accumulated the eremophilane-type sesquiterpene compound **3**, confirming it as a chemotaxonomic marker of the genus *Darksidea*. In contrast, two other eremophilanes, compounds **1** and **2**, were detected exclusively in the *Darksidea* clade 2. Furthermore, only a single lineage, *D. beta*, accumulated the tetramic acid derivatives **11**, **15**, **17**, and **18**. Species-specific accumulation was also observed for polyketides **12** and **16** in *D. phi*, and for **13** and **14** in *D. alpha*, respectively. Notably, differences in metabolite accumulation were also detected among isolates belonging to the same species. Of the two *D. phi* isolates (Fig. 1), only DS194 accumulated compounds **12** and **16**, while compounds **13** and **14** were produced by approximately one-third of the *D. alpha* isolates. Compounds **4**–**10** were detected in multiple species and likewise exhibited isolate-specific variation in metabolite production.

Considering these differences in metabolite accumulation among the fungal isolates, the most suitable isolates were selected for compound isolation, as detailed in the Experimental section (preparative HPLC isolation caption), yielding a total of 18 compounds.

2.4. Effects of compounds on Lemna minor growth

Specialized metabolites produced by endophytes may help counteract pathogenic competitors within the host plant (Li and Strobel, 2001; Schulz et al., 2002). Moreover, a finely tuned balance may exist between fungal virulence and host plant defense. To maintain this balance, both the host plant and its endophyte may produce specialized metabolites that modulate each other's metabolic processes and growth (Berthelot et al., 2016; Choi et al., 2004; Ko, 1994; Robeson and Strobel, 1982; Schulz et al., 2002) (Supplementary Table S7).

The *Lemna minor* assay was used here as a standardized and sensitive screening system for general plant growth-modulating activity rather than as a direct ecological model of *Darksidea*–host interactions. The *in vitro* plant growth-modulating activity of the isolated compounds was therefore evaluated using this assay (Vanhoutte et al., 2017), with frond number and total frond area used as indicators of plant growth. Of the 18 isolated compounds, compounds **5** and **16** were excluded from testing due to their limited availability.

Among the 16 compounds tested, compounds **3**, **7**, **8**, **10**–**13**, **15**, **17**, and **18** significantly reduced total frond area (Supplementary Fig. S31). The lowest concentrations producing a significant effect ranged from 10 to 150 μM. Most of these compounds also reduced frond number, whereas compounds **7** and **17** had no significant effect on this parameter. Among the ten active compounds, only petasol (**3**) has previously been reported to affect plant growth (Bunkers and Strobel, 1991;

Bunkers et al., 1990) (Supplementary Table S7). Further details on the observed activities and structure–activity relationships are provided in the Supplementary Material (page S62).

The relatively high proportion of active compounds among those tested warrants further investigation of their effects on grasses naturally hosting *Darksidea* species. Such studies will be essential to determine whether the plant growth-modulating activities observed in the standardized screening assay also have ecological relevance in natural *Darksidea*–host interactions.

Elucidating the molecular mechanisms underlying the activity of these compounds requires further investigation.

2.5. Antibacterial activity of compounds

The *in vitro* antibacterial activity of the isolated compounds was evaluated against methicillin-resistant (MRSA) and methicillin-susceptible (MSSA) strains of the Gram-positive bacterium *Staphylococcus aureus*, as well as against the Gram-negative bacteria *Escherichia coli* and *Pseudomonas aeruginosa*, using the broth microdilution assay. Among the 18 compounds tested, ascomycone A (**14**) and 6-deoxybostrycoidin (**10**) exhibited antibacterial activity, slightly inhibiting the growth of MRSA and MSSA strains. To the best of our knowledge, this is the first report of the antibacterial activity of compound **14** against *S. aureus* (details are provided in the Supplementary Material, page S63) (Lin et al., 2023; Moni et al., 2022).

3. Conclusions

The widely distributed dark septate endophytic fungal genus *Darksidea*, comprising 15 distinct lineages, including eight potentially novel taxa, was confirmed as a valuable source of specialized metabolites. In total, 18 compounds were identified and isolated, including four previously undescribed ones: two eremophilane-type sesquiterpenes (1-dehydroisopetasol and 3-petason) and two polyketides (mannuronyl-epicoccamide A and mannuronyl-epicoccamide D).

The plant growth-inhibitory activity of ten compounds was demonstrated for the first time using the *Lemna minor* growth assay. The relatively high proportion of active compounds identified through this standardized screening warrants further investigation of their effects on grasses naturally hosting endophytic fungi of the genus *Darksidea*. Such studies may reveal whether the observed plant growth-modulating activities contribute to the ecological interactions between *Darksidea* species and their grass hosts.

Two polyketide quinones, 6-deoxybostrycoidin and ascomycone A, exhibited mild antibacterial activity against both methicillin-resistant and methicillin-susceptible *Staphylococcus aureus* strains, with the antibacterial activity of ascomycone A against these strains being demonstrated for the first time.

4. Experimental

4.1. Fungal isolates and molecular identification

The *Darksidea* isolates were obtained from various host plants, ecosystems, and geographical regions (Supplementary Table S1) (Akhmetova et al., 2023; Glynou et al., 2016; Knapp et al., 2015, 2019; Romero-Jiménez et al., 2022).

For molecular phylogenetic identification, total DNA was extracted from the isolates using the NucleoSpin Plant II DNA Isolation Kit (Macherey-Nagel, Düren, Germany) following the manufacturer's instructions. The nrDNA ITS region was amplified and sequenced using the primer pair ITS1F (Gardes and Bruns, 1993) and ITS4 (White et al., 1990), when not available from previous studies. The enzyme applied for amplification was DreamTaq polymerase (Thermo Fisher Scientific, Vilnius, Lithuania). Sequencing was carried out by LGC Genomics (Berlin, Germany). The sequences were compiled using the Pregap4 and Gap4 tools of the Staden software package (Staden et al., 2000). The compiled sequences were deposited in GenBank (accession numbers provided in Supplementary Table S1) and compared to sequences available therein using the BLAST algorithm (Altschul et al., 1990).

For phylogenetic analyses, the sequences were aligned using the online version of MAFFT 7 (Katoh and Standley, 2013) applying the E-INS-i method. The alignment was edited in MEGA 7 (Kumar et al., 2016), and the edited alignment was 518 characters long.

Bayesian inference (BI) analysis was performed using MrBayes 3.2.7 (Ronquist et al., 2012), applying the GTR + G substitution model and the two-parameter Markov (Mk2 Lewis) model. In the case of the latter, four Markov chains were run for 10,000,000 generations, sampling every 1, 000th generation with a burn-in value set at 4000 sampled trees. For testing the support of branches, Bayesian posterior probabilities were calculated.

Maximum likelihood (ML) analysis was performed with the raxmlGUI 2.0 graphical implementation (Edler et al., 2021) of RAxML 8 (Stamatakis, 2014) applying the GTR + G substitution model. For testing the support of branches, ML bootstrap (BS) analysis with 1000 replicates in 10 runs was performed.

For both BI and ML analyses, *Lentithecium clioninum* (CBS 139694, accession number: NR154137) and *L. pseudoclioninum* (HHUF 29055, accession number: NR154108) served as multiple outgroups.

The phylogenetic tree was visualized and edited in MEGA 7 and deposited at the Figshare repository (https://doi.org/10.6084/m9.figshare.33353361).

4.2. Preparation and analysis of fungal culture extracts

Cultivation of Darksidea *isolates:* Fungal isolates were cultivated on Potato Dextrose Agar (PDA) medium (VWR, Hungary) for 3 weeks at room temperature in the dark. The resulting cultures, including both the growth medium and fungal mycelium, were lyophilized and subsequently pulverized.

Preparation of extracts for analysis and isolation: Lyophilized and pulverized fungal cultures (20.0 mg) were extracted with 3.0 mL of methanol at 60 °C for 30 min in 5 mL screw-capped vials. The extracts were centrifuged at 5000 rpm using a standard laboratory centrifuge, and the supernatants were subjected to HPLC-UV-MS/MS analysis. For compound isolation, pulverized culture material (approximately 2 g) was extracted three times with 15 mL of methanol at 60 °C for 30 min per extraction, using screw-capped vials. The supernatants from each extraction were centrifuged and pooled, then concentrated using a rotary vacuum evaporator. The dried residue was re-dissolved in 2.0 mL of methanol and centrifuged at 5000 rpm prior to preparative HPLC separation.

*Acid hydrolysis of epicoccamide A (**11**):* Compound **11** (8.0 mg) was heated in 2 mL of 2 M trifluoroacetic acid (TFA) at 100 °C for 60 min in a 5 mL screw-capped vial. The TFA was then removed under reduced pressure using a rotary evaporator, and the residue was partitioned between H_2O (2.0 mL) and CH_2Cl_2 (2.0 mL). The optical rotation of the aqueous phase containing D-mannose was measured: [α] +16.1 (c 0.2, H_2O). The CH_2Cl_2 phase was evaporated to dryness under reduced pressure. The resulting residue was dissolved in methanol (2.0 mL) and analyzed by HPLC-UV-HR-MS.

The NMR solvents, methanol-d_4 (99.80% D) and chloroform-*d* (99.80% D), were purchased from VWR International, Hungary. All other chemicals, such as acetonitrile, dichloromethane (CH_2Cl_2), distilled water, formic acid, methanol, and trifluoroacetic acid (TFA) (Reanal, Hungary), applied in the analysis were of analytical reagent grade of the highest purity available.

4.3. General experimental procedures

Analytical HPLC coupled with ultraviolet and high-resolution mass spectrometry detections: A Dionex Ultimate 3000 UHPLC system (SRD-

3400 solvent rack degasser, HPG-3400RS pump, WPS-3000TRS autosampler, TCC-3000RS column thermostat, 3000RS diode array detector (DAD)) coupled with an Orbitrap Q Exactive Focus Mass Spectrometer equipped with electrospray ionization (ESI) (Thermo Fisher Scientific, Waltham, MA, USA) were used for the separation and detection of compounds. HPLC separations were performed using a Kinetex C18 column (75 × 3 mm, 2.6 μm) (Phenomenex, USA). Eluents A (0.1% V/V formic acid) and B (acetonitrile:0.1% V/V formic acid; 80:20, V/V) were used for a gradient elution consisting of the following steps: 0.0 min, 20% B, 10.0 min, 70% B (linear gradient), 12.0 min, 90% B (linear gradient), 13.5 min, 90% B (isocratic); 14.0 min, 20% B (linear gradient), 16.0 min, 20% B (isocratic). Flow rate: 0.3 mL/min; column temperature: 25 °C, injected volumes: 1.0–5.0 μL. The ESI source was operated in switching mode (positive and negative ionization), the operation parameters were optimized using the built-in software as follows: spray voltage: 3500 V (+) and 2500 V (−), capillary temperature: 256 °C, sheath-, auxiliary- and spare-gases (N_2): 47.50, 11.25 and 2.25 arbitrary units, respectively. Full scans in *m/z* range between 100 and 1000 were acquired at a resolution of 70,000; the resolution of MS/MS scans was 35,000. Collision-induced dissociation (CID) energies were set between 10 and 45 eV. Fragmentation was performed using either (a) a data-independent acquisition (DIA) method with isolation windows of 100–300 *m/z*, 295–500 *m/z*, 495–700 *m/z*, 695–850 *m/z*, and 845–1000 *m/z*, or (b) manual selection of precursor ions with a 0.4 *m/z* isolation window. DAD spectra were recorded between 230 and 600 nm.

Preparative HPLC: A Pharmacia LKB HPLC system (2248 pumps, VWM 2141 UV detector) (Uppsala, Sweden) was used for the isolation of compounds. Preparative HPLC separations of compounds **3**, **4**, **6**, **7**, and **9** were performed on a Gemini C6-Phenyl (100 × 21.2 mm, 5 μm) column and those of compounds **1**, **2**, **5**, **8**, and **10**–**18** on a Gemini NX-C18 (150 × 21.2 mm, 5 μm) column (both columns were obtained from Phenomenex, USA). Gradient elutions were used with eluents A (0.1% V/V formic acid) and B (acetonitrile) at a flow rate of 5.0 mL/min, injecting 500 μL of the extracts. Different gradient elution programs were employed for the isolation of individual compounds, as detailed below: 0.0 min, 25% B, 50.0 min, 30% B (**1**, **2**); 0.0 min, 30% B, 30.0 min, 30% B, 50.0 min, 50% B (**3**, **4**, **6**, **7**); 0.0 min, 30% B, 60.0 min, 30% B (**5**); 0.0 min, 40% B, 15.0 min, 40% B, 20.0 min, 50% B, 50.0 min, 70% B, 70.0 min, 70% B (**8**, **10**, **13**, **14**); 0.0 min, 50% B, 15.0 min, 70% B, 18.0 min, 70% B (**9**); 0.0 min, 50% B, 10.0 min, 50% B, 40.0 min, 70% B, 65.0 min, 70% B (**11**, **15**, **17**, **18**); 0.0 min, 55% B, 10.0 min, 58.8% B, 40.0 min, 70% B (**12**, **16**).

Using these conditions, compounds were isolated as follows: 4.1 mg of compound **1** (t_R 26.2 min) and 6.4 mg of compound **2** (t_R 41.0 min) from 4.0 g of *Darksidea* clade 2, fungal isolate DS916); 16.8 mg of compound **3** (t_R 27.0 min) and 3.9 mg of compound **4** (t_R 30.1 min) from 5.0 g of *D. alpha*, fungal isolates DSE7/01, DSE7/15, DSE7/20, DS145, DS154, DS192, DS213, DS227, DS237, DS242, DS244, DS297, DS307, DS351, DS355, P6097; 0.9 mg of compound **5** (t_R 57.3 min) from 2.1 g of *D. alpha*, fungal isolates DSE7/04, DSE7/26, DSE7/28, DSE7/30, DSE7/Fest3; 8.1 mg of compound **6** (t_R 39.4 min) and 8.0 mg of compound **7** (t_R 45.4 min) from 6.8 g of *D. alpha*, fungal isolates DSE7/01, DSE7/04; 16.7 mg of compound **8** (t_R 35.2 min), 7.6 mg of compound **10** (t_R 40.1 min), 5.6 mg of compound **13** (t_R 52.0 min), and 8.2 mg of compound **14** (t_R 54.0 min) from 6.0 g of *D. alpha*, fungal isolate KG037; 6.0 mg of compound **9** (t_R 15.0 min) from 0.9 g of *D. alpha*, fungal isolate DS439; 20.6 mg of compound **11** (t_R 39.3 min), 23.0 mg of compound **15** (t_R 43.0 min), 20.3 mg of compound **17** (t_R 56.0 min), and 3.9 mg of compound **18** (t_R 61.2 min) from 4.0 g of *D. beta*, fungal isolate DSE7/11; 3.7 mg of compound **12** (t_R 31.3 min), and 1.0 mg of compound **16** (t_R 37.4 min) from 1.8 g of *D. phi*, fungal isolate DS194. Abbreviations of the fungal isolates correspond to those provided in Fig. 1 and Supplementary Table S1.

Nuclear magnetic resonance spectroscopy: The 1D ^{13}C (deptqsp), the 2D ^{1}H-^{13}C HSQC and ^{1}H-^{13}C HMBC NMR spectra of compound **5** were recorded in chloroform-*d* with a Bruker Avance NEO 500 MHz spectrometer (500.1 MHz for ^{1}H and 125.8 MHz for ^{13}C) equipped with a TCI cryo probe-head. The ^{1}H NMR spectra of compounds **8** and **14** were recorded on a Varian DDR spectrometer (599.9 MHz for ^{1}H and 150.9 MHz for ^{13}C) equipped with a dual 5 mm inverse detection gradient (IDPFG) probe-head using methanol-d_4 as the solvent. All the other 1D and 2D NMR spectra of the isolated compounds were recorded in chloroform-*d* and/or in methanol-d_4 at 25 °C using a Varian DDR Mercury Plus spectrometer (400.0 MHz for ^{1}H and 100.6 MHz for ^{13}C) equipped with a dual 5 mm inverse detection gradient (IDPFG) probe-head. Chemical shifts were referenced relative to the appropriate solvent resonance signals.

Circular dichroism (CD) spectroscopy: The CD spectra of the compounds were recorded in methanol using a Jasco J-815 spectropolarimeter (Jasco Inc., Tokyo, Japan). Each spectrum was obtained by averaging three accumulations, using a bandwidth of 1 nm, a step size of 0.2 nm, D.I.T. 2 sec., and a scan speed of 50 nm/min.

Optical rotation measurements: Optical rotations were measured at 25 °C on a Jasco P-200 polarimeter (Jasco Inc., Tokyo, Japan) using the sodium D line (589 nm). The isolated compounds were measured in methanol, whereas mannose obtained from the acid hydrolysis of epicoccamide A (**11**) was measured in H_2O.

Ultraviolet spectroscopy: λ_{max} and specific absorbance (log ε) values of compounds were determined in MeOH by a Jasco V-550 UV/Vis spectrophotometer (Jasco Inc., Tokyo, Japan).

Computational calculations: Electronic circular dichroism (ECD) spectra were calculated using the ORCA 5.0 quantum chemistry program package (Neese, 2022). Time-dependent density functional theory (TD-DFT) calculations were performed employing the CAM-B3LYP functional with the def2-TZVP basis set. The CPCM implicit solvent model was applied to simulate methanol as the solvent. Tight self-consistent field (TightSCF) convergence criteria were used. A total of 30 excited states (nroots = 30) were calculated for each compound. The RI approximation was applied with the def2/J auxiliary basis set.

1-dehydroisopetasol (**5**): yellowish, gelatinous oil; $[\alpha]_D^{25}$ +84.3 (*c* 0.15, MeOH); UV (MeOH) λ_{max} (log ε) 289.5 (3.34), 203.5 (3.42) nm; for ^{1}H NMR and ^{13}C NMR data, see Table 2; for HR-Orbitrap-MS data, see Table 1.

3-petason (**7**): yellowish, gelatinous oil; $[\alpha]_D^{25}$ +38.2 (*c* 0.2, MeOH); UV (MeOH) λ_{max} (log ε) 234.5 (3.73), 202.0 (3.39) nm; for ^{1}H NMR and ^{13}C NMR data, see Table 2; for HR-Orbitrap-MS data, see Table 1.

Mannuronyl-epicoccamide A (**15**): yellowish, gelatinous oil; $[\alpha]_D^{25}$ −61.1 (*c* 0.5, MeOH); UV (MeOH) λ_{max} (log ε) 283.5 (4.01), 225.0 (3.73) nm; for ^{1}H NMR and ^{13}C NMR data, see Table 3; for HR-Orbitrap-MS data, see Table 1.

Mannuronyl-epicoccamide D (**18**): yellowish, gelatinous oil; $[\alpha]_D^{25}$ −52.0 (*c* 0.2, MeOH); UV (MeOH) λ_{max} (log ε) 285.0 (3.82), 242.0 (3.81) nm; for ^{1}H NMR and ^{13}C NMR data, see Table 3; for HR-Orbitrap-MS data, see Table 1.

4.4. In vitro bioactivity assays

4.4.1. Lemna minor assay

Fronds of *Lemna minor* L. (clone 9441), long-term cultivated in a light chamber (16 h of light exposure) at 24 °C on liquid medium (Appenroth et al., 1996), were transferred two weeks before the test into Steinberg medium, which was changed after seven days (Naumann et al., 2007). Dilution series (2.0–150 μM) of isolated compounds were prepared using Steinberg medium, and the fronds were treated with 1.9 mL of these solutions (or the medium as a control) in 24-well plates for seven days under the light and thermal conditions of long-term cultivation. Subsequently, the fronds were counted, and their total area was measured in each well, using the software ImageJ and the screened images of plates (Schneider et al., 2012). Statistical analyses were conducted using the software Prism v.8.0.1 (GraphPad, USA). Normality of the datasets was

tested by applying the Shapiro-Wilk test; subsequently, one-way ANOVA was performed. The treatments were compared to the control with Tukey's *post hoc* test.

4.4.2. Antibacterial assay

Serial two-fold dilutions (200–0.39 μM) of compounds in Mueller-Hinton Broth (MHB) were tested on *Escherichia coli* ATCC 25922, *Pseudomonas aeruginosa* ATCC 27853, *Staphylococcus aureus* MRSA ATCC 33591, and MSSA ATCC 29213 strains. The bacterial suspensions were prepared in physiological saline solution with an optical density (OD) equal to 0.5 McFarland standard and were diluted 100-fold in MHB. Bacterial suspensions and test solutions (50-50 μL/well), bacterial suspensions and MHB (50-50 μL/well, growth control), or MHB alone (100 μL/well, sterile control) were pipetted into 96-well microtiter plates. The plates were incubated overnight at 37 °C. The minimal inhibitory concentration (MIC) values of the compounds were determined based on visual inspection and absorbance measurements at 595 nm (OD_{595nm}).

CRediT authorship contribution statement

Péter János Berek-Nagy: Writing – original draft, Visualization, Investigation, Data curation. **Dániel G. Knapp:** Investigation, Data curation. **Márta Kraszni:** Writing – original draft, Visualization, Methodology, Investigation. **Gergő Tóth:** Investigation. **Sándor Csíkos:** Investigation. **Petra Lengyel:** Investigation, Data curation. **Orsolya Dobay:** Investigation. **Galiya K. Akhmetova:** Investigation. **Aldabergen Kiyas:** Investigation, Data curation. **Vladimir Zabolotskich:** Investigation, Data curation. **Jose G. Maciá-Vicente:** Investigation, Data curation. **María-José Romero-Jiménez:** Investigation, Data curation. **Andrea Porras-Alfaro:** Investigation, Data curation. **Iñigo Zabalgogeazcoa:** Investigation, Data curation. **Gábor M. Kovács:** Writing – review & editing, Supervision, Software, Project administration, Methodology, Funding acquisition, Formal analysis, Data curation, Conceptualization. **Imre Boldizsár:** Writing – review & editing, Investigation, Data curation, Conceptualization.

Declaration of competing interest

The authors declare that they have no known competing financial interests or personal relationships that could have appeared to influence the work reported in this paper.

Acknowledgements

This work was supported by the National Research, Development and Innovation Office, Hungary (grants: NKFIH FK146930, K135712, K139026, VEKOP-2.3.3-15-2017-00020). This work was supported by the János Bolyai Research Scholarship of the Hungarian Academy of Sciences (G.T.) J.G.M.V. is supported by a Beatriz Galindo grant (BG23/00164) from the Spanish Ministry of Science, Innovation and Universities (MICIU). The work was also supported by the National Science Foundation (Award 1457002 to A. P-A.). Any opinion, findings, and conclusions or recommendations expressed in this material are those of the authors (A. P-A.) and do not necessarily reflect the views of the U.S. National Science Foundation or of the U.S. Federal government. The authors gratefully acknowledge Dr. Péter Horváth and Dr. Gergely Dombi (Department of Pharmaceutical Chemistry, Semmelweis University) for performing the CD spectroscopic analyses and interpreting the resulting spectral data.

Appendix A. Supplementary data

Supplementary data to this article can be found online at https://doi.org/10.1016/j.phytochem.2026.115066.

Data availability

Data will be made available on request.

References

Akhmetova, G.K., Knapp, D.G., Özer, G., O'Donnell, K., Laraba, I., Kiyas, A., Zabolotskich, V., Kovács, G.M., Molnár, O., 2023. Multilocus molecular phylogenetic-led discovery and formal recognition of four novel root-colonizing *Fusarium* species from northern Kazakhstan and the phylogenetically divergent *Fusarium steppicola* lineage. Mycologia 115, 16–31. https://doi.org/10.1080/00275514.2022.2119761.

Aldridge, D.C., Turner, W.B., 1970. Metabolites of *Helminthosporium monoceras*: structures of monocerin and related benzopyrans. J. Chem. Soc. C Org. 2598–2600. https://doi.org/10.1039/J39700002598.

Altschul, S.F., Gish, W., Miller, W., Myers, E.W., Lipman, D.J., 1990. Basic local alignment search tool. J. Mol. Biol. 215, 403–410. https://doi.org/10.1016/S0022-2836(05)80360-2.

Appenroth, K., Teller, S., Horn, M., 1996. Photophysiology of turion formation and germination in *Spirodela polyrhiza*. Biol. Plant. (Prague) 38, 95–106. https://doi.org/10.1007/BF02879642.

Berek-Nagy, P.J., Tóth, G., Bősze, S., Horváth, L.B., Darcsi, A., Csíkos, S., Knapp, D.G., Kovács, G.M., Boldizsár, I., 2021. The grass root endophytic fungus *Flavomyces fulophazii*: an abundant source of tetramic acid and chlorinated azaphilone derivatives. Phytochemistry 190, 112851. https://doi.org/10.1016/j.phytochem.2021.112851.

Berthelot, C., Leyval, C., Foulon, J., Chalot, M., Blaudez, D., 2016. Plant growth promotion, metabolite production and metal tolerance of dark septate endophytes isolated from metal-polluted poplar phytomanagement sites. FEMS Microbiol. Ecol. 92, fiw144. https://doi.org/10.1093/femsec/fiw144.

Bunkers, G., Kenfield, D., Strobel, G., Sugawara, F., 1990. Structure-activity relationships of the eremophilanes produced by *Drechslera gigantea*. Phytochemistry 29, 1471–1474. https://doi.org/10.1016/0031-9422(90)80103-N.

Bunkers, G.J., Strobel, G.A., 1991. A proposed mode of action for green island induction by the eremophilane phytotoxins produced by *Drechslera gigantea*. Physiol. Mol. Plant Pathol. 38, 313–323.

Cheng, Z., Zhao, J., Liu, D., Proksch, P., Zhao, Z., Lin, W., 2016. Eremophilane-type sesquiterpenoids from an *Acremonium* sp. fungus isolated from deep-sea sediments. J. Nat. Prod. 79, 1035–1047. https://doi.org/10.1021/acs.jnatprod.5b01103.

Choi, G.J., Park, J., Kim, H.T., Lee, S., Choi, J., Hong, K., Cho, K.Y., Kim, J., 2004. Phytotoxicity of endophytic fungi and characterization of a phytotoxin isolated from *Gliocladium catenulatum* from *Pinus densiflora*. Kor. J. Mycol. 32, 8–15. https://doi.org/10.4489/KJM.2004.32.1.008.

Daengrot, C., Rukachaisirikul, V., Tansakul, C., Thongpanchang, T., Phongpaichit, S., Bowornwiriyapan, K., Sakayaroj, J., 2015. Eremophilane sesquiterpenes and diphenyl thioethers from the soil fungus *Penicillium copticola* PSU-RSPG138. J. Nat. Prod. 78, 615–622. https://doi.org/10.1021/np5005328.

Deshmukh, S.K., Dufossé, L., Chhipa, H., Saxena, S., Mahajan, G.B., Gupta, M.K., 2022. Fungal endophytes: a potential source of antibacterial compounds. J. Fungi 8, 164. https://doi.org/10.3390/jof8020164.

Edler, D., Klein, J., Antonelli, A., Silvestro, D., 2021. raxmlGUI 2.0: a graphical interface and toolkit for phylogenetic analyses using RAxML. Methods Ecol. Evol. 12, 373–377. https://doi.org/10.1111/2041-210X.13512.

Gakuubi, M.M., Ching, K.C., Munusamy, M., Wibowo, M., Liang, Z., Kanagasundaram, Y., Ng, S.B., 2022. Enhancing the discovery of bioactive secondary metabolites from fungal endophytes using chemical elicitation and variation of fermentation media. Front. Microbiol. 13, 898976. https://doi.org/10.3389/fmicb.2022.898976.

Gardes, M., Bruns, T.D., 1993. ITS primers with enhanced specificity for basidiomycetes – application to the identification of mycorrhizae and rusts. Mol. Ecol. 2, 113–118. https://doi.org/10.1111/j.1365-294X.1993.tb00005.x.

Glynou, K., Ali, T., Buch, A., Kia, S.H., Ploch, S., Xia, X., Çelik, A., Thines, M., Maciá-Vicente, J.G., 2016. The local environment determines the assembly of root endophytic fungi at a continental scale. Environ. Microbiol. 18, 2418–2434. https://doi.org/10.1111/1462-2920.13112.

Hardoim, P.R., van Overbeek, L.S., Berg, G., Pirttilä, A.M., Compant, S., Campisano, A., Döring, M., Sessitsch, A., 2015. The hidden world within plants: ecological and evolutionary considerations for defining functioning of microbial endophytes. Microbiol. Mol. Biol. Rev. 79, 293–320. https://doi.org/10.1128/MMBR.00050-14.

Jacobs, J., Tehrani, K.A., De Kimpe, N., 2011. A survey of synthetic routes towards 2-azaanthraquinones. Tetrahedron 67, 9459–9471. https://doi.org/10.1016/j.tet.2011.10.017.

Kanai, Y., Tatsumi, Y., Tokiwa, T., Watanabe, Y., Fujimaki, T., Ishiyama, D., Okuda, T., 2005. F2928-1 and -2, new antifungal antibiotics from *Cladobotryum* sp. J. Antibiot. 58, 507–513. https://doi.org/10.1038/ja.2005.68.

Katoh, K., Standley, D.M., 2013. MAFFT multiple sequence alignment software version 7: improvements in performance and usability. Mol. Biol. Evol. 30, 772–780. https://doi.org/10.1093/molbev/mst010.

Knapp, D.G., Imrefi, I., Boldpurev, E., Csíkos, S., Akhmetova, G., Berek-Nagy, P.J., Otgonsuren, B., Kovács, G.M., 2019. Root-colonizing endophytic fungi of the dominant grass *Stipa krylovii* from a Mongolian steppe grassland. Front. Microbiol. 10, 2565. https://doi.org/10.3389/fmicb.2019.02565.

Knapp, D.G., Kovács, G.M., Zajta, E., Groenewald, J.Z., Crous, P.W., 2015. Dark septate endophytic pleosporalean genera from semiarid areas. Persoonia 35, 87–100. https://doi.org/10.3767/003158515X687669.

Knapp, D.G., Pintye, A., Kovács, G.M., 2012. The dark side is not fastidious – dark septate endophytic fungi of native and invasive plants of semiarid sandy areas. PLoS One 7, e32570. https://doi.org/10.1371/journal.pone.0032570.

Ko, B., 1994. Synthesis and phytotoxic activities of (8S, 9S, 11R)-(-)-monocerin and (9S, 11R)-(+)-fusarentin 4, 5-dimethyl ether. Agric. Chem. Biotechnol. 37, 402–408.

Kobayashi, H., Meguro, S., Yoshimoto, T., Namikoshi, M., 2003. Absolute structure, biosynthesis, and anti-microtubule activity of phomopsidin, isolated from a marine-derived fungus *phomopsis* sp. Tetrahedron 59, 455–459. https://doi.org/10.1016/S0040-4020(02)01566-1.

Kumar, S., Stecher, G., Tamura, K., 2016. MEGA7: molecular evolutionary genetics analysis version 7.0 for bigger datasets. Mol. Biol. Evol. 33, 1870–1874. https://doi.org/10.1093/molbev/msw054.

Le, D.H., Takenaka, Y., Hamada, N., Tanahashi, T., 2013. Eremophilane-type sesquiterpenes from cultured lichen mycobionts of *Sarcographa tricosa*. Phytochemistry 91, 242–248. https://doi.org/10.1016/j.phytochem.2012.01.009.

Li, J.Y., Strobel, G.A., 2001. Jesterone and hydroxy-jesterone antioomycete cyclohexenone epoxides from the endophytic fungus *Pestalotiopsis jesteri*. Phytochemistry 57, 261–265. https://doi.org/10.1016/S0031-9422(01)00021-8.

Lin, C., Huang, R., Liu, J., Li, H., Zhu, L., Huang, X., Ding, B., Liu, L., Huang, H., Tao, Y., 2023. Antibacterial polyketides isolated from the marine-derived fungus *Fusarium solani* 8388. J. Fungi 9, 875. https://doi.org/10.3390/jof9090875.

Maciá-Vicente, J.G., Shi, Y., Cheikh-Ali, Z., Grün, P., Glynou, K., Kia, S.H., Piepenbring, M., Bode, H.B., 2018. Metabolomics-based chemotaxonomy of root endophytic fungi for natural products discovery. Environ. Microbiol. 20, 1253–1270. https://doi.org/10.1111/1462-2920.14072.

Mandyam, K., Jumpponen, A., 2005. Seeking the elusive function of the root-colonising dark septate endophytic fungi. Stud. Mycol. 53, 173–189. https://doi.org/10.3114/sim.53.1.173.

Mitova, M.I., Lang, G., Blunt, J.W., Cummings, N.J., Cole, A.L.J., Robinson, W.T., Munro, M.H.G., 2006. Cladobotric acids A–F: new cytotoxic polyketides from a New Zealand *Cladobotryum* sp. J. Org. Chem. 71, 492–497. https://doi.org/10.1021/jo051883l.

Moni, F., Saifullah, N., Afroz, F., Rony, S.R., Sharmin, S., Shahinuzzaman, A.D.A., Al-Mansur, M.A., Al-Reza, S.M., Sohrab, M.H., 2022. Antibacterial and cytotoxic compounds from endophyte *Fusarium solani* isolated from *Centella asiatica* (L.). J. Biol. Act. Prod. Nat. 12, 436–449. https://doi.org/10.1080/22311866.2022.2144947.

Namikoshi, M., Kobayashi, H., Yoshimoto, T., Hosoya, T., 1997. Phomopsidin, a new inhibitor of microtubule assembly produced by Phomopsis sp. isolated from coral reef in Pohnpei. J. Antibiot. (Tokyo). 50, 890–892. https://doi.org/10.7164/antibiotics.50.890.

Naumann, B., Eberius, M., Appenroth, K., 2007. Growth rate based dose–response relationships and EC-values of ten heavy metals using the duckweed growth inhibition test (ISO 20079) with *Lemna minor* L. clone St. J. Plant Physiol. 164, 1656–1664. https://doi.org/10.1016/j.jplph.2006.10.011.

Neese, F., 2022. Software update: the ORCA program system–version 5.0. WIREs Comput. Mol. Sci. 12, e1606. https://doi.org/10.1002/wcms.1606.

Nisa, H., Kamili, A.N., Nawchoo, I.A., Shafi, S., Shameem, N., Bandh, S.A., 2015. Fungal endophytes as prolific source of phytochemicals and other bioactive natural products: a review. Microb. Pathog. 82, 50–59. https://doi.org/10.1016/j.micpath.2015.04.001.

Opatz, T., Kolshorn, H., Thines, E., Anke, H., 2008. Ascomycones A–C, heptaketide metabolites from an unidentified ascomycete. J. Nat. Prod. 71, 1973–1976. https://doi.org/10.1021/np800570w.

Parisot, D., Devys, M., Barbier, M., 1989. 5-deoxybostrycoidin, a new metabolite produced by the fungus *Nectria haematococca* (Berk. and Br.) Wr. Z. Naturforsch. B 44b, 1473–1474. https://doi.org/10.1515/znb-1989-1125.

Porras-Alfaro, A., Bayman, P., 2011. Hidden fungi, emergent properties: endophytes and microbiomes. Annu. Rev. Phytopathol. 49, 291–315. https://doi.org/10.1146/annurev-phyto-080508-081831.

Porras-Alfaro, A., Herrera, J., Sinsabaugh, R.L., Odenbach, K.J., Lowrey, T., Natvig, D.O., 2008. Novel root fungal consortium associated with a dominant desert grass. Appl. Environ. Microbiol. 74, 2805–2813. https://doi.org/10.1128/AEM.02769-07.

Qin, C., Lin, X., Lu, X., Wan, J., Zhou, X., Liao, S., Tu, Z., Xu, S., Liu, Y., 2015. Sesquiterpenoids and xanthones derivatives produced by sponge-derived fungus *Stachybotry* sp. HH1 ZSDS1F1-2. J. Antibiot. 68, 121–125. https://doi.org/10.1038/ja.2014.97.

Robeson, D.J., Strobel, G.A., 1982. Monocerin, a phytotoxin from *Exserohilum turcicum* (≡ *Drechslera turcica*). Agric. Biol. Chem. 46, 2681–2683. https://doi.org/10.1080/00021369.1982.10865494.

Rodriguez, R.J., White Jr., J.F., Arnold, A.E., Redman, R.S., 2009. Fungal endophytes: diversity and functional roles. New Phytol. 182, 314–330. https://doi.org/10.1111/j.1469-8137.2009.02773.x.

Romero-Jiménez, M., Rudgers, J.A., Jumpponen, A., Herrera, J., Hutchinson, M., Kuske, C., Dunbar, J., Knapp, D.G., Kovács, G.M., Porras-Alfaro, A., 2022. *Darksidea phi*, sp. Nov., a dark septate root-associated fungus in foundation grasses in North American Great Plains. Mycologia 114, 254–269. https://doi.org/10.1080/00275514.2022.2031780.

Ronquist, F., Teslenko, M., van der Mark, P., Ayres, D.L., Darling, A., Höhna, S., Larget, B., Liu, L., Suchard, M.A., Huelsenbeck, J.P., 2012. MrBayes 3.2: efficient Bayesian phylogenetic inference and model choice across a large model space. Syst. Biol. 61, 539–542. https://doi.org/10.1093/sysbio/sys029.

Rudgers, J.A., Fox, S., Porras-Alfaro, A., Herrera, J., Reazin, C., Kent, D.R., Souza, L., Chung, Y.A., Jumpponen, A., 2022. Biogeography of root-associated fungi in foundation grasses of North American plains. J. Biogeogr. 49, 22–37. https://doi.org/10.1111/jbi.14260.

Saikkonen, K., Faeth, S.H., Helander, M., Sullivan, T.J., 1998. Fungal endophytes: a continuum of interactions with host plants. Annu. Rev. Ecol. Syst. 29, 319–343. https://doi.org/10.1146/annurev.ecolsys.29.1.319.

Sappapan, R., Sommit, D., Ngamrojanavanich, N., Pengpreecha, S., Wiyakrutta, S., Sriubolmas, N., Pudhom, K., 2008. 11-Hydroxymonocerin from the plant endophytic fungus *Exserohilum rostratum*. J. Nat. Prod. 71, 1657–1659. https://doi.org/10.1021/np8004024.

Schardl, C.L., Grossman, R.B., Nagabhyru, P., Faulkner, J.R., Mallik, U.P., 2007. Loline alkaloids: currencies of mutualism. Phytochemistry 68, 980–996. https://doi.org/10.1016/j.phytochem.2007.01.010.

Schneider, C.A., Rasband, W.S., Eliceiri, K.W., 2012. NIH Image to ImageJ: 25 years of image analysis. Nat. Methods 9, 671–675. https://doi.org/10.1038/nmeth.2089.

Schoch, C.L., Seifert, K.A., Huhndorf, S., Robert, V., Spouge, J.L., Levesque, C.A., Chen, W., Fungal Barcoding Consortium, 2012. Nuclear ribosomal internal transcribed spacer (ITS) region as a universal DNA barcode marker for Fungi. Proc. Natl. Acad. Sci. U. S. A. 109, 6241–6246. https://doi.org/10.1073/pnas.1117018109.

Schoeffel, E., Link, K.P., 1933. Isolation of α- and β, *d*-mannuronic acid. J. BioI. Chern. 100, 397–405. https://doi.org/10.1016/S0021-9258(18)75957-7.

Schulz, B., Boyle, C., Draeger, S., Römmert, A., Krohn, K., 2002. Endophytic fungi: a source of novel biologically active secondary metabolites. Mycol. Res. 106, 996–1004. https://doi.org/10.1017/S0953756202006342.

Schwarz, M., Köpcke, B., Weber, R.W.S., Sterner, O., Anke, H., 2004. 3-Hydroxypropionic acid as a nematicidal principle in endophytic fungi. Phytochemistry 65, 2239–2245. https://doi.org/10.1016/j.phytochem.2004.06.035.

Sieber, T.N., Grünig, C.R., 2013. Fungal root endophytes. In: Eshel, A., Beeckman, T. (Eds.), Plant Roots: the Hidden Half, fourth ed. CRC Press, Boca Raton, Florida, USA, pp. 1–49. chapter 38.

Staden, R., Beal, K.F., Bonfield, J.K., 2000. The staden package, 1998. In: Misener, S., Krawetz, S.A. (Eds.), Bioinformatics Methods and Protocols. Methods in Molecular Biology^{tm}, vol. 132. Humana Press, Totowa, New Jersey, USA, pp. 115–130. https://doi.org/10.1385/1-59259-192-2:115.

Stamatakis, A., 2014. RAxML version 8: a tool for phylogenetic analysis and post-analysis of large phylogenies. Bioinformatics 30, 1312–1313. https://doi.org/10.1093/bioinformatics/btu033.

Stodůlková, E., Man, P., Kuzma, M., Černý, J., Císařová, I., Kubátová, A., Chudíčková, M., Kolařík, M., Flieger, M., 2015. A highly diverse spectrum of naphthoquinone derivatives produced by the endophytic fungus *Biatriospora* sp. CCF 4378. Folia Microbiol. 60, 259–267. https://doi.org/10.1007/s12223-014-0366-7.

Sugama, K., Hayashi, K., Nakagawa, T., Mitsuhashi, H., Yoshida, N., 1983. Sesquiterpenoids from *Petasites fragrans*. Phytochemistry 22, 1619–1622. https://doi.org/10.1016/0031-9422(83)80099-5.

Tabata, Y., Hatsu, M., Kurata, Y., Miyajima, K., Tani, M., Sasaki, T., Kodama, Y., Tsuruoka, T., Omoto, S., 1997. PF1092A, B and C, new nonsteroidal progesterone receptor ligands produced by *Penicillium oblatum* II. Physico-chemical properties and structure elucidation. J. Antibiot. 50, 309–313. https://doi.org/10.7164/antibiotics.50.309.

Tenhaken, R., Voglas, E., Cock, J.M., Neu, V., Huber, C.G., 2011. Characterization of GDP-mannose dehydrogenase from the brown alga Ectocarpus siliculosus providing the precursor for the alginate polymer. J. Biol. Chem. 286, 16707–16715. https://doi.org/10.1074/jbc.M111.230979.

Vanhoutte, I., De Mets, L., De Boevre, M., Uka, V., Di Mavungu, J.D., De Saeger, S., De Gelder, L., Audenaert, K., 2017. Microbial detoxification of deoxynivalenol (DON), assessed via a *Lemna minor* L. bioassay, through biotransformation to 3-epi-DON and 3-epi-DOM-1. Toxins 9, 63. https://doi.org/10.3390/toxins9020063.

Wang, C., Li, J., Yang, R., Zhao, Y., Cheng, Y., Zhang, Z., He, L., 2014. Petasins from the rhizomes of *Ligularia fischeri* and its derivatives. Rec. Nat. Prod. 8, 156–164.

Wangun, H.V.K., Dahse, H., Hertweck, C., 2007. Epicoccamides B–D, glycosylated tetramic acid derivatives from an *Epicoccum* sp. associated with the tree fungus *Pholiota squarrosa*. J. Nat. Prod. 70, 1800–1803. https://doi.org/10.1021/np070245q.

White, T.J., Bruns, T., Lee, S., Taylor, J., 1990. Amplification and direct sequencing of fungal ribosomal RNA genes for phylogenetics. In: Innis, M.A., Gelfand, D.H., Sninsky, J.J., White, T.J. (Eds.), PCR Protocols: a Guide to Methods and Applications. Academic Press, New York, New York, USA, pp. 315–322.

Wright, A.D., Osterhage, C., König, G.M., 2003. Epicoccamide, a novel secondary metabolite from a jellyfish-derived culture of *Epicoccum purpurascens*. Org. Biomol. Chem. 1, 507–510. https://doi.org/10.1039/B208588G.

Xie, F., Luan, X., Gao, Y., Xu, K., Lou, H., 2020. Cytotoxic heptaketides from the endolichenic fungus *Ulospora bilgramii*. J. Nat. Prod. 83, 1623–1633. https://doi.org/10.1021/acs.jnatprod.0c00108.